J Civil Struct Health Monit (2012) 2:1–16
DOI 10.1007/s13349-011-0013-9

ORIGINAL PAPER

Condition assessment of a heritage arch bridge using a novel model updation technique

Pradipta Banerji · Sanjay Chikermane

Received: 18 September 2011 / Accepted: 12 November 2011 / Published online: 30 November 2011

Abstract The bridge network on Indian Railways comprises a large number of masonry arch bridges, a significant number of which are more than 100 years old. The traffic intensities and the loads that are imposed on these structures are significantly higher than those for which they were designed. A significant proportion of these arch bridges is still in good condition and might be structurally adequate for the increased traffic conditions and need not be replaced. A robust identification and assessment procedure is, therefore, critical to enable proper decisions to be taken by railway authorities for managing their arch bridges. A comprehensive monitoring of a 75-year-old heritage stone masonry arch was undertaken. The measured responses were used along with a generated finite element model for structural system identification. The finite element model was updated to estimate the properties and associated degradation of the materials in the masonry arch. The condition of the structure was then estimated to be satisfactory as the converged parameters were well within the expected ranges for the materials in question. The updated model can also be used to reliably check the adequacy of the bridge for future design loads. As the monitoring cost is just a fraction of the replacement cost of the system, this process shows promise of being able to be used to validate the existing infrastructure of stone masonry arch railway bridges and to optimize their replacement.

Keywords Stone masonry arch · Model updating · Condition assessment · Structural health monitoring · Multi-parameter optimization · Parameter estimation

P. Banerji (✉) · S. Chikermane
Indian Institute of Technology, Bombay, India
e-mail: pbanerji@iitb.ac.in

1 Introduction

Masonry arch bridges are perhaps the most common type of bridge structures constructed around the world in the nineteenth and the early part of the twentieth century, as stated by Orban [16]. India also has many masonry arch bridges, built of either stone or brick masonry with lime or lean cement mortar, on its rail and road networks. Since these bridges were built close to a century ago, and are today subjected to loads that are far in excess of what they may have been designed for, it is imperative to assess the current condition and future load carrying capacity of such bridges. Most of these bridges are heritage structures, and if any retrofitting is required it needs to be done while keeping in mind the heritage of the bridge.

In this paper, structural health assessment of an actual railway bridge is presented, where a combination of site measurements and a numerical analysis is used to assess the current condition. The experimental phase of the project involved monitoring the displacements and strains at various locations in a span under a specific design train and for actual traffic conditions. The numerical phase involves creating a finite element model that accurately considers the structural behavior of the arch, and estimating the material properties in the model using a novel model updating technique that ensures convergence between the experimental and numerical response values. The postulation in this paper is that the current condition of the bridge can be assessed by comparing these estimated material properties against the expected or originally tested values of the properties.

There has, in the knowledge of the authors, no previous attempt made to identify the individual material properties of all components of a stone masonry arch bridge, which include the stone voussoirs, the mortar and the fill at

different locations as a multi-parameter system identification. Most attempts at system identification of stone masonry arches have concentrated upon identification of single parameters. Also, there has been no previous attempt made, in the knowledge of the authors, to use the strain response measurements as a model updating criteria in arch bridges.

2 Numerical and material modeling basis

The problem of creating a realistic model of a masonry arch has been attempted by several researchers. There have been a large number of modeling ideologies chosen by them. Tóth et al. [20] give a good account of the state of the art of the numerical modeling of masonry arches.

The behavior of stone masonry arches has been shown by Heyman [11] as corresponding to a set of basic assumptions:

(a) stone has no tensile strength;
(b) stone has effectively infinite compressive strength;
(c) sliding of stone blocks cannot happen over each other.

Based upon these approaches, a thrust line approach to analysis of stone masonry arches was developed and the upper and lower bounds of safety were formulated. Pippard and Baker [17] showed that at a point just before collapse, four hinges were formed that were mechanistically equivalent to a four bar chain capable of deformation with a single degree of freedom. Pippard et al. [18] also concluded that since masonry was fundamentally an NTR (no-tension-resistance) structure, small imperfections in construction would always convert any arch into a system that already has three hinges present. This in itself is not alarming, as it is only the formation of the fourth hinge which transforms the structure into a mechanism.

While these lower bound and upper bound methods are applicable to estimate the strength of an arch, they do not give adequate information at different load levels, and hence these need to be augmented by more sophisticated numerical models to remove these shortfalls.

As reported by Tóth et al. [20], although continuum-based FEM models have widely been applied for the 2D or 3D analysis of masonry structures and definitely have their role in masonry analysis, masonry is fundamentally a discrete system. The mechanical behavior is determined partly by the characteristics of the blocks and of the discontinuities between them (mortar or frictional contact), and partly by the geometrical arrangement of the discontinuities. Sophisticated FEM approaches are able to reflect this discrete nature and have been explored by several researchers, a good review of which is given by Boothby [4] and more recently by Tóth et al. [20] and Audenaert et al. [2].

Crisfield [6] has attempted to identify the stone Young's modulus, but the primary motive in that experiment was to identify the collapse loads. This study was one of the pioneering studies in modeling stone masonry using finite elements and is of historical importance. It also validates the approach of using a two-dimensional element formulation to model a masonry arch that has no spandrel beams. The stone in the arch modeled by Crisfield was similar to that under consideration, and the Young's modulus taken by Crisfield was seen to be in the same range as the one that finally converged (within a 10% range). He modeled the stone masonry arch as a two-dimensional element having a unit width using a plane stress approach for the masonry and a plane strain approach for the fill to estimate the collapse load and the corresponding deflections. The fill–masonry interface was assumed to be a free slip interface. The fill in this approach was modeled to have a Mohr–Coulomb yield criterion. The modulus of elasticity of the fill was taken as 40 MPa and the angle of internal friction was kept at 30°. The modulus of elasticity of the masonry, was taken as first the stone value of 14.1 GPa and then again as a value 1/3rd of this to account for the stone masonry combined behavior. A better correspondence with experimental data on collapse load was obtained by taking the higher modulus for masonry, although it has been pointed out that similar convergence could be attained by changing the fill properties. Since the objective was to identify the collapse load, which is seen to be independent of the modulus of elasticity if effects of geometric non-linearity are ignored, the model was not further updated. Both the approaches depicted assume a smeared model, where the stone masonry is modeled as a single material.

Bayraktar et al. [3] also modeled the voussoir–mortar assembly as a homogeneous material for a two span arch and attempted to identify the natural frequencies by adjusting the boundary conditions. The parameter chosen for this was the acceleration data from the ambient conditions.

Fanning and Boothby [8] modeled an arch bridge using a smeared model and considering a specific solid element in a standard commercially available FE software. They recommended a smeared modulus of elasticity of 5–15 GPa for stone masonry using cut stones with thin joints. For a bridge with ashlar limestone masonry in the arch and joints less than 1-cm thick, they modeled the masonry to have a modulus of elasticity of 10 GPa. The fill was modeled as a Drucker–Prager material having a frictional contact with the underlying stone masonry by giving appropriate values of frictional coefficients in the normal and tangential directions. The modulus of elasticity of the fill was modeled to be 1.5 GPa, and the Poisson's ratio was kept at 0.3. The other parameters were taken as 1 kPa for the cohesion value, and an angle of 44.43° for the dilatancy angle and 44.43° for the angle of internal friction. The displacement

was measured at the haunch and the crown, and reasonably good convergence between the simulated results and the recorded data was seen for displacement response.

Ford et al. [9] modeled the masonry as a series of elements having a plane strain formulation connected at pre-determined points, which were regularly introduced. These connections were modeled as a set of springs, which had a tension cutoff, in the sense that there was a limiting tensile strength after which separation would occur. The fill was modeled as a linear elastic material, connected by a set of springs having a similar tensile cutoff, but with a different limiting tensile value. On checking the model, it was found that the fill limited the expected hinge formation. This was then dealt with by reducing the value of the fill modulus rather than creating an elasto-plastic model due to considerations of numerical costs. The interface was also modeled using a set of shear panel elements with a high modulus of elasticity to insure that sliding did not occur within the voussoirs.

It has been shown by Cavicchi and Gambarotta [5] that the plane strain assumption is reasonably valid and gives accurate results for masonry bridges which are not narrow. In bridges where the width of the barrel is of more or less the same scale as the span, the plane strain assumption gives reasonably accurate results. This assumption is also supported by Gilbert [10].

Fanning and Boothby [8] and Ford et al. [9] have shown that material modeling has an extremely important role to play in the numerical representation of masonry arches. Masonry is known to be a brittle material, and hence homogenous representation of masonry is inappropriate. The properties of the stone, mortar and fill material are important parameters in modeling the material, and the joints between these individual components of the arch are important in its numerical representation.

The E value of sandstone is taken by Lukaszewski [14] to be in the range of 7.9–19.4 GPa, with lower values for coarse-grained stones (7.9–14.8 GPa) and higher values for fine-grained stones (14.2–19.4 GPa). In the model prepared by Crisfield [6], the sandstone was experimentally found to have a value of 14.1 GPa. The stone used in the bridge under consideration was medium-grained sandstone and hence the range of values considered was from 12 to 20 GPa.

Opinions differ on what the E value of fill should be among different researchers. Tóth et al. [20] state that the UIC (Union Internationale des Chemins de fer) code estimates dense sand to be about 200 MPa, loose sand to be 20 MPa, medium clay to be 10 MPa and soft clay to be 1 MPa. Thus, the E value of the graded fill in the masonry arch considered in this paper is therefore between 20 and 200 MPa depending upon its compaction and composition. The haunch fill composition is low-grade cement/lime concrete, and the E value is taken to be higher. The was been modeled as a Drucker–Prager material according to Fanning and Boothby [8], but the angle of internal friction was kept as 30°, as considered by Crisfield, to be more in accordance with the current condition of the fill. Day [7] gives the internal friction angle of silts to be between 28° and 34° for medium to dense compactions, so a value of 30° is reasonable for the kind of soil under consideration.

As per Karantzikis [13] and Spyrakos [19], the value of the modulus of elasticity for soil behind abutments varies from a shear modulus of 70–280 MPa depending upon the compaction. As per the Eurocode 8, part 5 specifications, the Young's modulus of soil should be considered as three times the shear modulus. So the Young's modulus values range from 210 MPa for loose soils to 840 MPa for well-compacted soils.

For the present model, the Young's modulus of the mortar has to be converted into an equivalent spring stiffness as the mortar is modeled using non-linear springs. The starting value for small strains is considered as:

$$\text{stiffness} = {(E_{\text{mortar}} \times A_{\text{arch}})}/{(l \times \text{n})} \quad (1)$$

The value of A is the area of the stone interface. For a plane strain model, having a unit width, A is taken as the thickness of the stone voussoir, which for the present model is 0.54 m. The value of "l" is the thickness of the mortar joint, which is on an average found out to be 12.5 mm in this case. The n in the above equation is the number of springs used over the voussoir depth, which in the present model is 7. The conversion ratio between the Young's modulus of mortar and the initial stiffness of the spring is hence worked out to be 6.17. Hence,

$$\text{stiffness}(N/m) = 6.17 \times E_{\text{mortar}}\left(N/m^2\right) \quad (2)$$

Jiang and Esaki [12] gave a constitutive model of the mortar by substituting it with springs and contact elements having a stiffness of 7.64 GPa/m for a 150-year-old masonry arch in tuff stone masonry. This value was used by Tóth et al. [20] in computing the response of a multi-span arch.

The stiffness of the springs considered depends upon the Young's modulus of the mortar. As given in McNary and Abrams [15], the different types of mortar defined by ASTM according to the volume proportions of cement:lime:sand were: Type M (1:0.25:3), Type S (1:0.5:4.5), Type N (1:1:6) and Type O (1:2:9). Although the exact proportion of the mortar used in this bridge is not known, the bridge description and documentation mention that a weak cement lime mortar was used. The type O mortar hence seems to best fit the description of the mortar used for the building. McNary and Abrams [15] did a series of tests of the mortars which were commonly used. For the mortar designated as type O, for a cement–water ratio of 0.51, the compressive strength was found to be 3.4 MPa, the Young's modulus for this mortar under no confining stress was about 1.6 GPa and the Poisson's ratio was approximately 0.1–0.2. This mortar, while still exhibiting brittle failure, showed substantially

increased strain taking capacity and failed at strains almost thrice that at which the stronger type M mortar failed. Since the exact composition of the mortar used for the bridge is unknown, the values estimated by McNary and Abrams are considered as a mean value. The values of the Young's modulus for the mortar are, thus, varied between 0.5 and 2 GPa, as an expected range of this parameter.

3 Modeling strategy and problem definition

3.1 Description of the bridge

The bridge is a four-span stone masonry arch, as shown in Fig. 1. The arch bridge was constructed in 1934. The stone used, as stated earlier, was locally procured medium-grained sandstone with the joints made of weak cement lime mortar. The fill was a well-compacted silty-sand fill as described earlier. The arch does not exhibit any problems of drainage or local masonry degradation. The stone masonry is formed using reasonably thin joints of 12.5-mm thickness. The visual inspection of the arch shows a good overall condition of the structure.

3.2 Site data analysis

The site response data considered here were the vertical displacement at the crown, the lateral displacements at the pier and abutment springing points and strains along the barrel at all the three locations given in Fig. 1. All

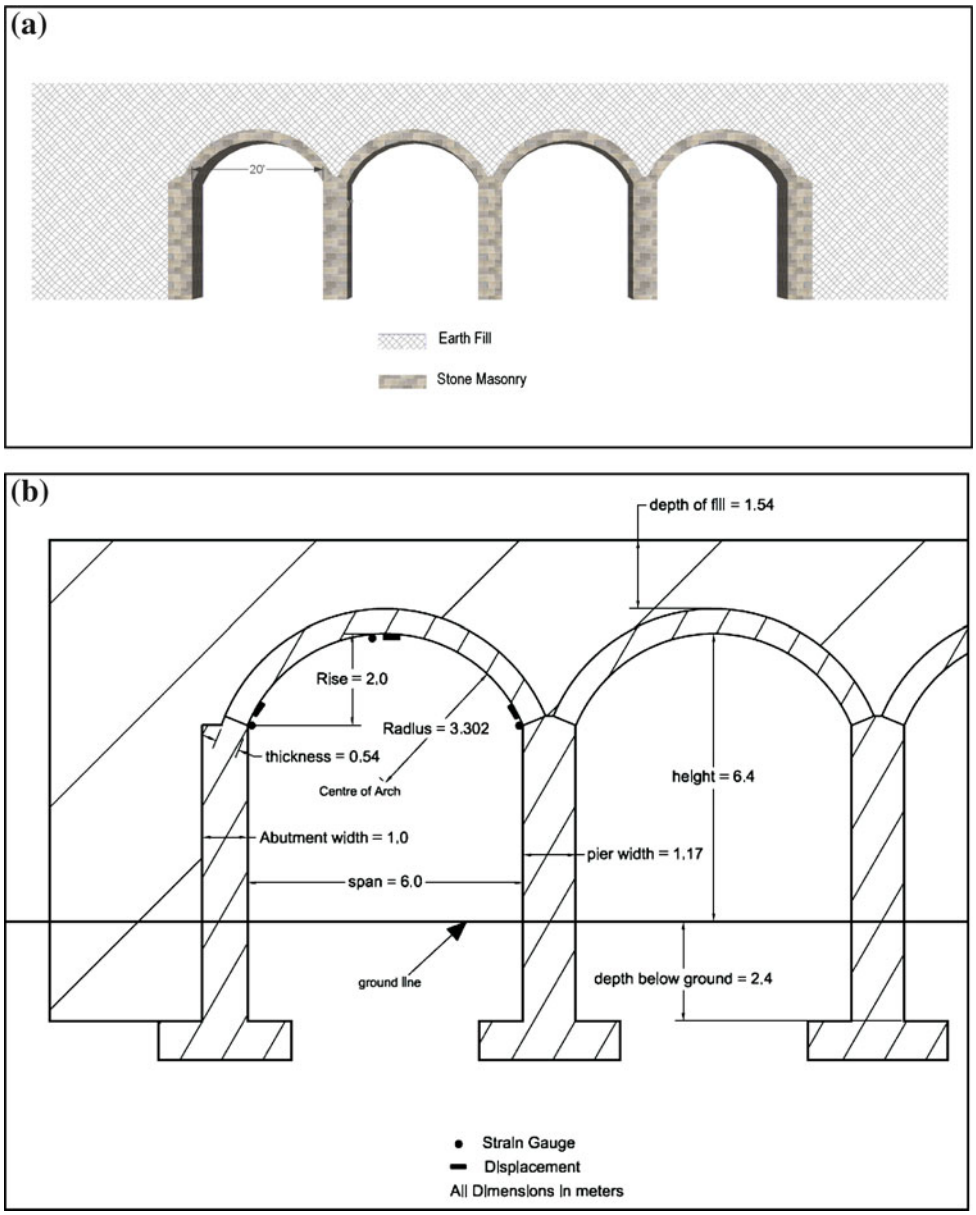

Fig. 1 Details of arch. **a** Overview of the arch; **b** Overview of instrumented span

responses were measured along three lines across the barrel—the downstream and upstream ends and the centerline. The strains were recorded directly from the stone and not across the mortar joints. This was done because the strain measured across a joint fundamentally comprises both rigid body movement and strain due to stone deformations. The strain gauge cannot differentiate between deformation and rigid body movements separately. It is thus difficult to isolate the deformation-based strain from the apparent strains, especially as in the case of rigid body movements, the apparent strains would be significantly higher than those due to deformations alone. The strain measured when placing the sensor on the stone gives the deformation-based response only and has no rigid body component in it. Also, the strain values are significant as seen in Fig. 2a and, as the signal strength is strong, there is not much contamination of the signal due to noise.

The displacements were recorded using conductive plastic linear potentiometer of travel 50 mm and resistance 5 kΩ.

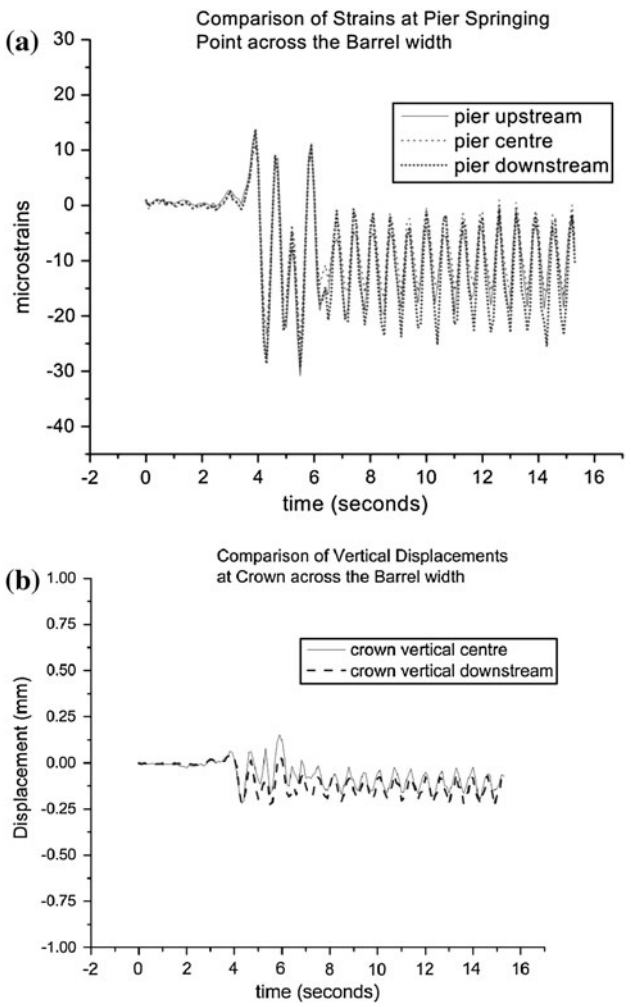

Fig. 2 Comparison of typical response values across the width of the arch

The strains were measured using long gauge-length electric resistance strain gauges of resistance 120 Ω and gauge length 120 mm. The analog data were routed to a conditioning amplifier, which had a least count display set at 0.01 mm for displacement data and 0.05 micro-strains for the strain data.

The site data shows insignificant dynamic effects for response values monitored, as shown in Table 1. This is corroborated from site recordings, where different speed runs show almost identical response values.

The arch response data were recorded for several events. These were for entire design train runs at varying speeds over the bridge. The design train comprised two locomotives having six axles of axle loads 20.5 tons each. These locomotives were followed by 58 wagons having four axles each and having a varying but known weight between 21 and 23 tons. The rear end of the train comprised two more locomotives of the same description as above to allow movements in both directions.

For a sample run of the train, moving at a constant speed of 45 kmph, the response time history for sensors across the barrel for two representative responses are shown in Fig. 2. It is seen that the response time histories are practically identical. Since there was not much variation of values along the barrel width, any of these sets could be taken for model validation. In the present paper, the response data from the center of the barrel, for all the responses shown in Fig. 1, were considered for model validation and updating. In these time histories, it should be noted that the first few seconds correspond to an empty span and the time histories used for further validation with the numerical model neglects this time span and considers the time histories only when the train comes on the span. Since the bridge under consideration has a 6 m span and a width of 4.87 m, the bridge is reasonably wide and hence the plane strain assumption is valid, based on past research. Hence, it is reasonable that the arch could be modeled using plane strain elements without significant loss of accuracy.

3.3 Numerical model

In the present model, modeling of the individual stones is done as per the site-measured geometric values. The mortar joints have been modeled again as measured from the site, and the pre-determined planes of weakness were modeled at these mortar stone interfaces. The deviation from the geometry modeling ideology of Ford, et al. is that the planes of weakness are as obtained from exact site measurements. The choice of the element formulation of the stone blocks is a plane strain formulation, as mentioned above. The mortar is modeled as a set of non-linear springs having virtually no tensile strength. A negligible value of 1 kN force was applied as a tension lift-off to ensure numerical convergence. This value is, however, small

Table 1 Site-recorded responses for different train speeds

	Crawling speed (<5 kmph)	Slow speed (20 kmph)	Design speed (65 kmph)
Vertical displacement at the center of the span (mm)	−0.30	−0.27	−0.34
Lateral displacement at the springing point pier (mm)	0.24	0.27	0.24
Lateral displacement at the springing point abutment (mm)	−0.04	−0.04	−0.04
Longitudinal strain along the arch at crown (microstrain)	22.1	21.4	19.4
Longitudinal strain along the arch at the springing point pier (microstrain)	−24.62	−24.83	−25.68
Longitudinal strain along the arch at the springing point abutment (microstrain)	−24.0	−22.2	−23.2

enough that there is practically no tensile strength for the non-linear springs. The shear panels were introduced with a modulus of elasticity equal to that of the stone masonry. These were introduced to control the sliding capacity of the blocks. The fill was modeled to have a Drucker–Prager failure criterion, as mentioned earlier. The fill masonry interface was modeled using a series of contact elements with frictional resistance. The spaces between the haunches were thus modeled to have a higher modulus of elasticity than the rest of the fill. The fill behind the abutment was also modeled to have a higher modulus of elasticity as compared to the basic fill, as this fill is traditionally very well compacted, as mentioned earlier.

The model was created using the software ANSYS v5.5 [1]. The element chosen for modeling the stone voussoir and the fill was the PLANE42 element with the sub-choice of plane strain formulation. The mortar was modeled using the elements CONTA178 to model the springs and the element SHELL28 to model the shear panels. The finite element model is shown in Fig. 3. It should be noted here that this numerical model is valid for the service load conditions considered here, and not necessarily for computation of collapse loads, which is not attempted in this study. The solution considers non-linear effects and large deflections and therefore requires an iterative solution where the stiffness matrix is updated for geometry and stress stiffening. The convergence criteria have been taken as the force criteria with a convergence norm of 0.001. This implies that the solution is deemed to have converged when the out-of-balance forces are less than 0.1% of the applied forces. Typically, the load is incremented in a minimum number of ten load steps. However, in certain situations, the number of

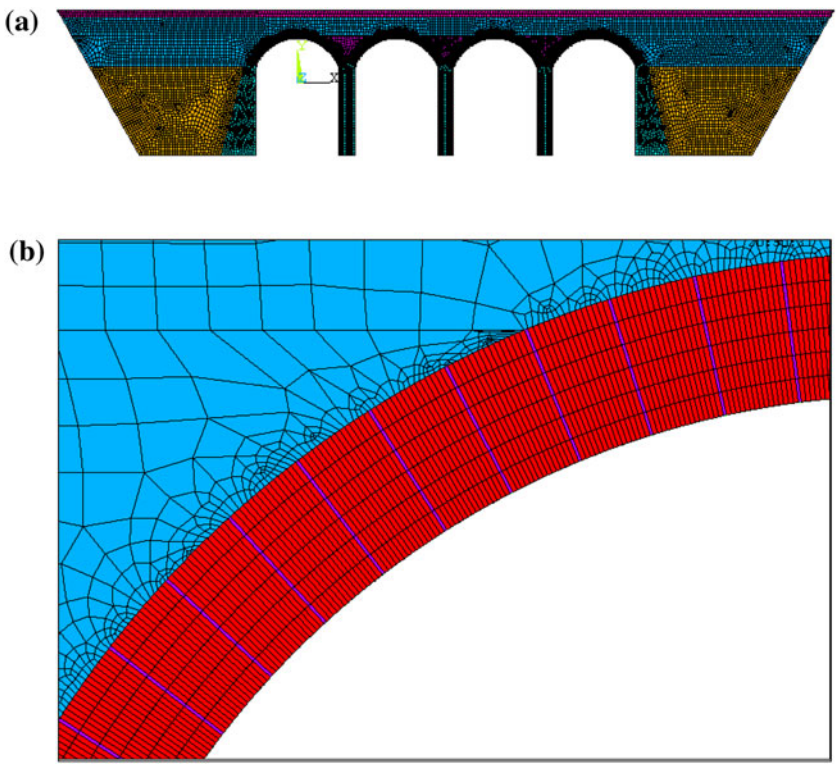

Fig. 3 **a** Details of the finite element model and **b** Blowup of the model to show the arch ring

iterations required for convergence was fairly large, although the maximum number of iterations for each load step was defined as 100, to avoid non-convergence issues.

Since the finite element numerical model is fairly complex with a large number of degrees of freedom, where analysis needs a significant amount of computation time, the entire design train was not run on the bridge. However, the two locomotives comprising 12 axles and eight wagons comprising 32 axles were run. It is expected that the pattern of results generated from this case would be repeated through the entire load run. This set of loads was moved with an incremental time of 0.005 s to correspond with the measured sampling rate. The entire bridge of four spans was subjected to these loads. The self-weight was activated in the first few load steps and then kept constant through the rest of the run. The results generated thus comprised the self-weight loads and the train loads. The self-weight response was then subtracted from these results to give the response for comparison with the site-measured data.

3.4 Parameter identification and model updating

The internal angle of friction for the soil fill at abutment and above the arch was considered to be 30°. This was because it was not very clear whether varying this parameter would provide us any significant information on the state of the arch. From a preliminary analysis, it was seen that over entire ranges of acceptable values of the other materials, the responses were relatively unaffected by changes in the frictional contact between voussoir and fill. This is expected, as the sliding between the voussoirs and fill is not expected at service load conditions. The co-efficient of friction was hence kept at the lower bound value of 0.4 and remained unchanged over the entire model updating exercise. Heyman's hypothesis [11] states that within the limit of the service loads, the masonry needs to be constrained so as to not slide against each other. However, in some cases, it is possible for a snap-through failure to occur. The value of 1 MPa is the ultimate shear strength prescribed for mortar in the Indian Railway bridge code, and thus this value has been taken for modeling purposes. There were no signs of visible fracture planes in the masonry from a physical inspection and hence this value has not been changed further. The numerical model of the arch also did not show any signs of snap-through failure at the service loads.

The finite element numerical model created is, therefore, a multi-parameter model with the significant parameters being shown in Table 2. In this table, the acceptable ranges are defined as discussed in the previous section on material modeling. The initial parameter values for the parameter identification and sensitivity results have also been identified in this table.

The range of the expected value changes is significantly large, and with five parameters, it would take a very large computational effort to use any of the standard multi-parameter optimization algorithms to come to a converged solution, and, as shown later, the converged solution need not necessarily be a global optimum solution. Thus, an innovative algorithm is proposed for model updating, which has been shown to be relatively computationally efficient, while converging consistently to a solution with a lower error norm.

The algorithm works on identifying the most critical variables and using design-sensitivity analysis to estimate their hierarchy for consideration. The five-parameter problem is thus broken down into various sets of either single or two-parameter problems, which are computationally far more tractable. The algorithm is shown in Fig. 4.

The design train run was simulated on the numerical model and a full transient dynamic analysis was performed. The peak values of individual responses were monitored and the load cases corresponding to these were solved using static analysis. The results were almost identical and hence the slices corresponding to individual peak responses, solved statically, could be considered as being representative of the peak response during the run. For different response parameters, different slices were considered as the peaks did not occur identically at the same spatial load representation. The error was computed as follows:

Table 2 Structural parameters used for modeling

	Voussoir	Fill	Fill (haunch)	Contact (voussoir)	Fill (abutment)	Contact (fill)
Start Young's modulus	16 GPa	110 MPa	3 GPa	1,250 MPa	530 MPa	110 MPa
Poisson's ratio	0.19	0.19	0.19	–	0.19	0.19
Density (kg/m^3)	2,200	1,800	2,200	–	1,800	–
Start contact/frictional stiffness	–	–		67.8 GN/m[a]	–	0.4 (coeff of friction)[b]
Tensile lift-off	–	–		1 kN	–	100 MN[c]
Acceptable ranges	12–20 GPa	20–200 MPa	1–5 GPa	500–2,000 MPa	20–850 MPa	0.4–0.6

[a] This corresponds to Young's modulus of 1.25 GPa

[b] Sliding of fill over voussoirs not dominant at service loads

[c] High value of tension lift-off provided to prevent separation. Sliding is, however, possible

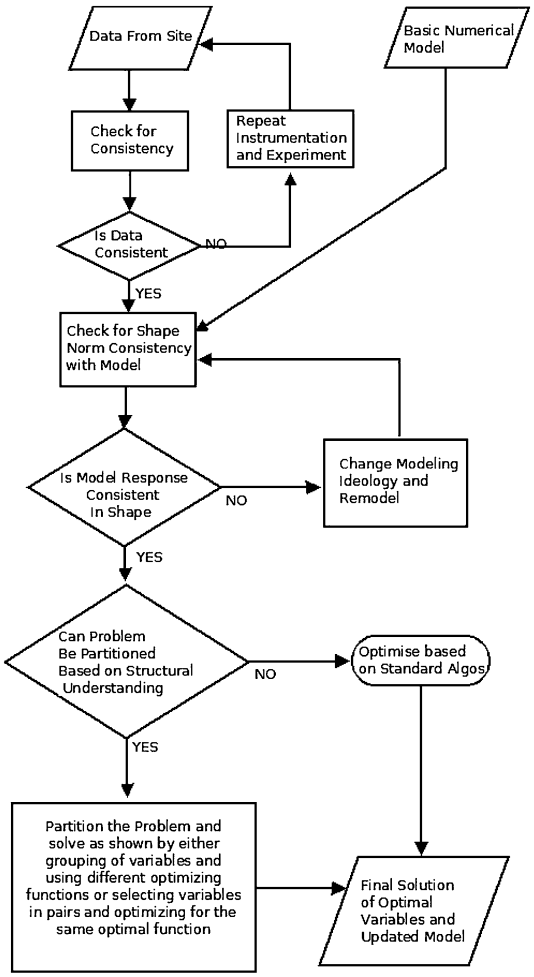

Fig. 4 Overview of model updating algorithm

$$\frac{(\text{peaknumericalresponse} - \text{peaksiteresponse})}{\text{peak site response}} = \text{error} \quad (3)$$

Thus, the comparisons between the numerical model and site results were done using this peak norm.

The errors are weighted depending upon the shape correlation factors and a weighted root mean square norm considered. This is done to generate a single cost function to be optimized. This procedure ensures that all the responses are considered for model updating, while also ensuring that the weights end up giving higher dependence on well-correlated responses as against lesser correlated ones. The shape correlation factor (scf) is given by:

$$\text{scf} = \frac{\sum_{i=1}^{N} u[i]v[i]}{\left(\sum_{i=1}^{N}(u[i])^2\right)^{1/2}\left(\sum_{i=1}^{N}(v[i])^2\right)^{1/2}} \quad (4)$$

where N is the number of data points for a complete dynamic run. The shape correlation factors give a normalized correlation between the numerical response u[i] and site-measured data v[i]. The weights considered for computing a weighted root mean square (WRMS) value are the square of shape correlation factors for each sensor. The values of the scf for different sensors are given in Table 3.

Table 3 Correlation factors between numerical model and site responses

Sensor	Correlation factor
Horizontal displacement at the abutment springing point	0.816
Vertical displacement at the crown	0.949
Horizontal displacement at the pier springing point	0.931
Intrados strain at the abutment springing point	0.945
Intrados strain at the crown	0.872
Intrados strain at the pier springing point	0.953

3.5 Individual parameter sensitivity

The WRMS value of the error was computed over all the response quantities. Each individual parameter was varied over the entire range of acceptable values and the variation of the WRMS error norm monitored. It is assumed that the minimal WRMS error norm would occur when the parameter values are closest to their "true value". Sensitivity studies for each individual parameter are shown in Fig. 5. In these plots, the values of the parameters assumed constant are at their mean value, which is the central value of the parameter range considered.

From Fig. 5, it can be seen that the WRMS error norm changes significantly over the range of change of the parameters, i.e., it is sensitive to each parameter. Also, from the graphs, it can be seen that the problem is generally well posed and that the graphs generated are generally smooth (with the exception of the haunch fill). An attempt was made to identify the most significant of these parameters.

A classification is made based on the range of WRMS error for variation of each parameter over the entire range of its possible values as given in Table 1. These are given, with ranking based on the WRMS error range or sensitivity, in Table 4. From the sensitivity graphs, a naïve assumption is to consider all the parameters at their individual minimal error norm values. This gives a weighted root mean square peak norm error of 0.24 and is based on single parameter optimization.

It is interesting to note how each of the parameters affects individual response error values as given by Eq. (3). The plots in Fig. 6 show the variations of the individual response for variation of each parameter over its allowable range. The error ranges for individual responses are tabulated in Table 5. This illustrates the problem of

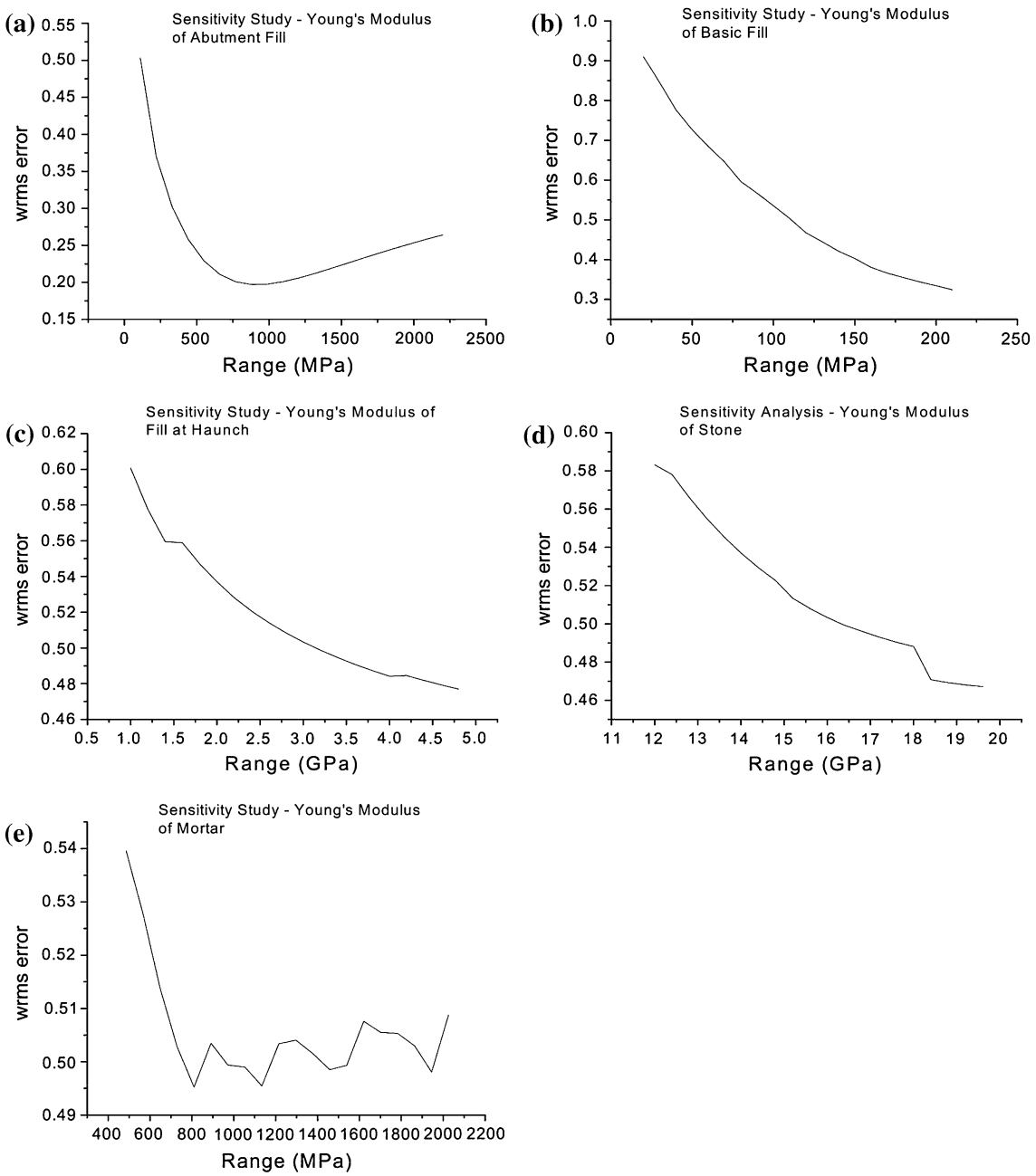

Fig. 5 Individual sensitivity studies for parameter variation on response RMS error

classification based on individual responses, as sensitivity of each response varies with each parameter and it is impossible to uniquely classify the parameters. This highlights the reason why the WRMS error norm has been used in this study for sensitivity classification.

From Table 4, the most significant parameters seem to be the Young's modulus of the abutment fill and the Young's modulus of the basic fill. The modulus of elasticity of mortar is seen to be the least significant of the five parameters considered.

3.6 Combined parameter sensitivity

From the earlier analysis, the two most significant parameters chosen are the Young's modulus of the abutment fill and the Young's modulus of basic fill. The other parameters are changed to be at their relative minimum from the individual sensitivity analysis. So the Young's modulus of stone voussoirs is changed from the start model value of 16–18.4 GPa, that of mortar from the start value of 1,250 MPa to the new value of 810 MPa and that of the

Table 4 Ranking of individual parameters based upon WRMS error ranges

Rank	Parameter	Minimum WRMS error over range of parameter values	Maximum WRMS error over range of parameter values	WRMS error range	Value of parameter at minimum WRMS error
1	Young's Modulus—basic fill	0.32	0.91	0.59	200 MPa
2	Young's modulus—abutment fill	0.20	0.50	0.30	880 MPa
3	Young's modulus—haunch fill	0.60	0.48	0.12	4.8 GPa
4	Young's modulus—stone voussoir	0.58	0.47	0.11	18.4 GPa
5	Stiffness of mortar—Young's modulus	0.54	0.49	0.05	0.81 GPa

haunch fill from 3 GPa to 4.8 GPa. The two significant parameters are then varied over the entire range. The weighted error norm is computed for each numerical run and graphed as a surface. The minimal point of the surface corresponds to the best converged model. This is given in Fig. 7.

There are three possibilities for the minimal point. The first is if it is in the interior of the parameter space with a global minima being defined at this point. In this case, both the parameters are assumed to have converged and the point in the parameter space gives the values of these. The second case is if one of the parameters is in the interior of the parameter space and the other at a boundary. In this case, the parameter having the minima at an interior point is assumed to have converged only. The second parameter is then iterated again with the next parameter chosen from the basis of the individual sensitivity analysis. The third case is if both the parameters are on the boundary. In this case, the algorithm is deemed to have failed or the parameter space needs to be augmented accordingly and the algorithm run again.

The best fit converged values correspond to a value of 850 MPa for the Young's modulus of the abutment fill, and a value for the Young's modulus of the basic fill which did not show any decided trough. From these, the value of 850 MPa for the abutment fill elastic modulus is frozen. For the second round, the primary variable considered is the Young's modulus of the basic fill and the secondary variable is the Young's modulus for voussoir stones. The Young's modulus of abutment fill is changed to 850 MPa. Other values remain at their present status. The result of this analysis is shown in Fig. 8.

The best fit converged values correspond to a value of 170 MPa for the Young's modulus of the basic fill. The Young's modulus of the stone voussoir does not show a decided trough and hence are carried forward into the next analysis. The next two-parameter analysis is done for the haunch fill and the Young's modulus of voussoirs and the modulus of elasticity of the haunch fill, as shown in Fig. 9.

The final variation of the error norm with the Young's modulus of mortar is given in Fig. 10. The final values of the parameters after the model updating exercise are shown in Table 6. They are compared with the results from a standard software optimization solution, which gives the converged solution having a significantly larger error norm than the proposed algorithm. The standard software optimization was done in the ANSYS software using the optimizing module inbuilt in the software. The gradient search method was taken for optimization with the program default controls. The cost function to be optimized was taken as identical to the WRMS error function defined earlier.

It is possible that for models of this nature, there may be more than one solution which gives similar degrees of error norms as the optimization algorithm may converge to the local minima. The methodology proposed addresses this issue by showing that starting at different points in the parameter space generates convergence to identical points in the solution space. This establishes the robustness of the technique: that independent of the starting point, the global minima points are attained.

Although the present algorithm is run from the starting points of the parameters as being the mean points, even if the parameter space constitutes values of the parameters being kept at the boundary values of the acceptable ranges, the algorithm converges over a two-pass system to the identical point identified earlier. This makes the algorithm independent of the initial parameter value choices and establishes the robustness of the algorithm. Taking the parameters at their mean values, however, significantly improves the solution time, and hence it is recommended that this approach be followed.

From Table 6, it is seen that the values of fill at all locations are excellent, indicating an extremely well-consolidated fill. The values of fill behind the abutment and the basic fill value are almost at the maximum indicated for these parameters. However, there is a degradation of value of the mortar Young's modulus from an expected value of 1.6 GPa. On the whole, the behavior of the arch would not change significantly, as the dependence on fill is significantly higher than on the mortar. The fill has probably improved in value over the years of service due to possible compaction. The value of Young's modulus of stone voussoir is estimated at about 13.2 GPa, which seems reasonable for the kind of stone used.

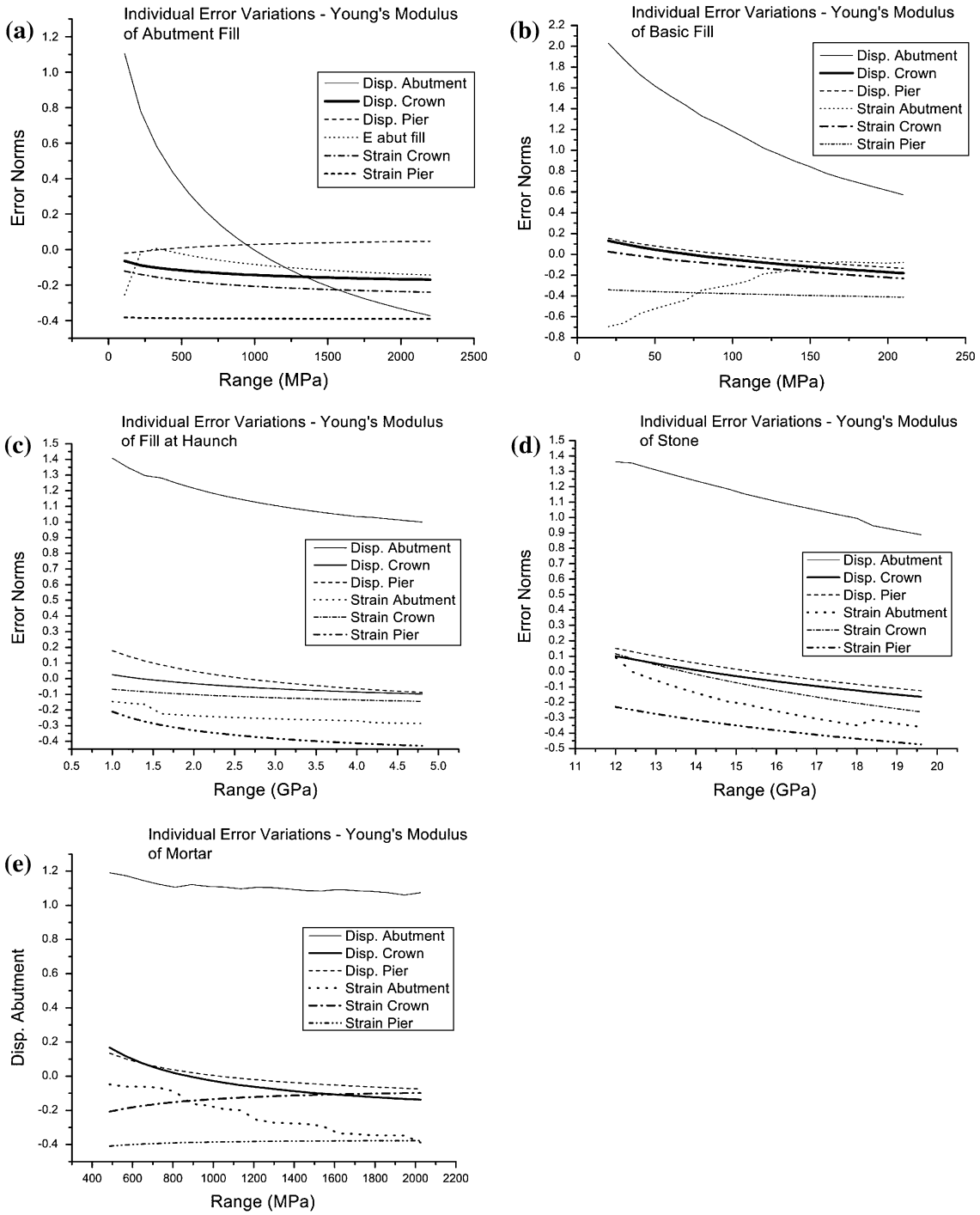

Fig. 6 Variations of individual response quantities to parameter changes

4 Analysis results

The updated finite element numerical model is then used to generate the time histories of various response quantities, given in Fig. 1, measured on site at the centerline across the barrel due to the design train runs. Some typical analysis results for a particular run of the design train are compared with measured responses for that run.

4.1 Results at crown

At the crown, the response quantities monitored were the vertical displacement at the crown and the longitudinal

Table 5 Effect of parameter changes on individual response error ranges

Parameter	Response				
	Young's modulus—basic fill	Young's modulus—abutment fill	Young's modulus—haunch fill	Young's modulus—voussoir	Young's modulus—mortar
Displacement at abutment	1.46	1.48	0.41	0.47	0.13
Displacement at crown	0.31	0.11	0.12	0.26	0.30
Displacement at pier	0.29	0.07	0.27	0.28	0.21
Strain at abutment	0.62	0.26	0.14	0.45	0.34
Strain at crown	0.26	0.12	0.08	0.38	0.11
Strain at pier	0.07	0.01	0.22	0.24	0.03
Average error range	0.50	0.34	0.21	0.35	0.19

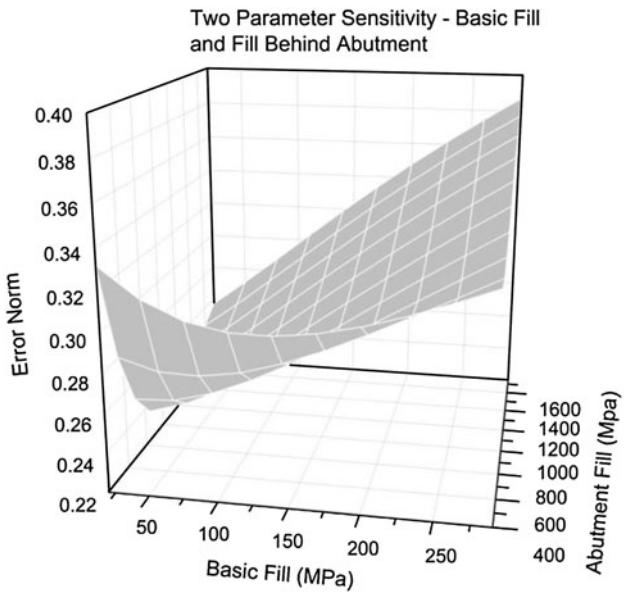

Fig. 7 Variation of WRMS error norm for the joint variation of two parameters—abutment fill and basic fill modulii

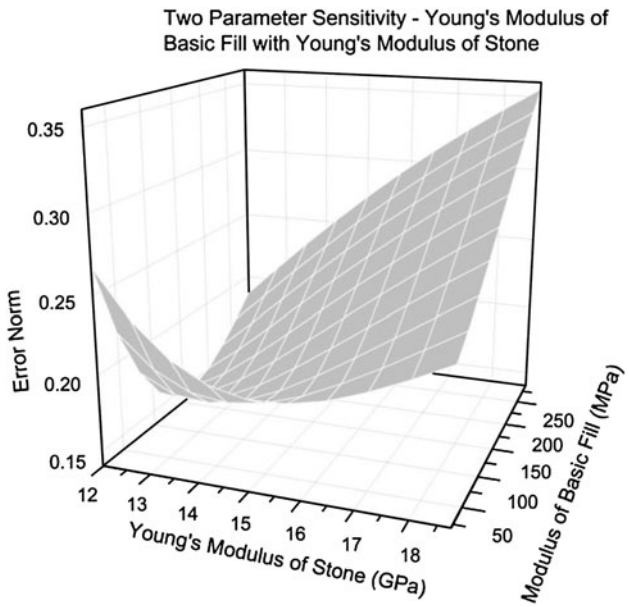

Fig. 8 Variation of WRMS error norm for the joint variation of two parameters—basic fill and stone voussoir modulii

strain along the barrel on the stone. These gave good comparisons with the measured site data. The graphs of these are shown in Fig. 11.

4.2 Results at the pier springing point

At the pier springing point, the responses monitored were the lateral displacement of the arch and the longitudinal strain at the barrel. These were found to be in excellent concurrence with the measured site data as shown in Fig. 12.

4.3 Results at abutment springing point

At the abutment springing point, the responses monitored were the lateral displacement of the arch and the longitudinal strain at the barrel. The strain was found to be in excellent concurrence with the measured site data. The lateral displacement correlation, however, was relatively poorer. At this location, the measured displacements are small enough to have noise have a significant effect, or there may have been sensor malfunction. This parameter was thus not considered in the convergence criteria to

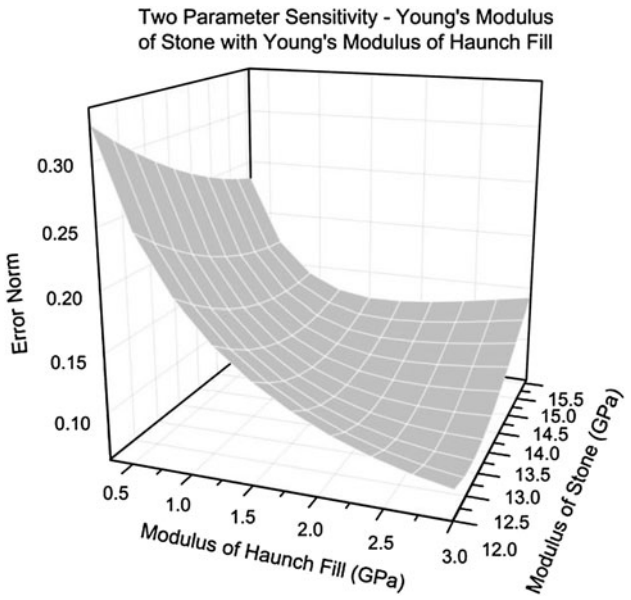

Fig. 9 Variation of WRMS error norm for the joint variation of two parameters—haunch fill and stone voussoir modulii

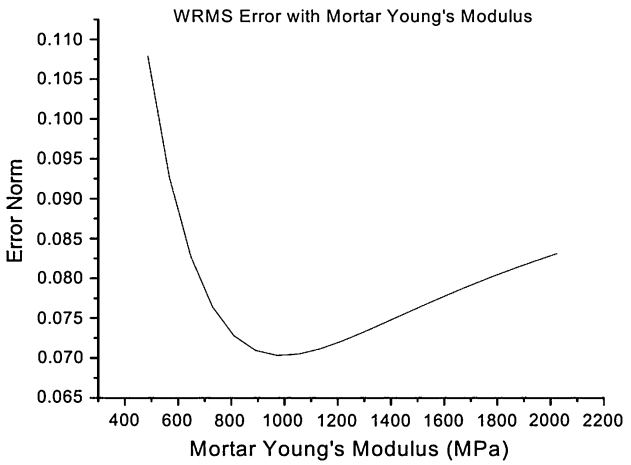

Fig. 10 Variation of WRMS error norm with Young's modulus of mortar

generate the material properties. The results are shown in Fig. 13.

4.4 Other results

The displacement and strain contours, using the site-validated and updated numerical model, are shown for the arch ring in Fig. 14. The contours are considered at a load step that corresponds to the load case where one locomotive has completely crossed the test span and the other locomotive has the first set of its axles centrally placed on the test span. The rest of the train has not yet entered the test span.

After getting a good fit of the numerical model with the site-recorded data, the model is then subject to the proposed increased loading. The design checks are done as per the current Indian Railway loading standards. The response expected from the bridge to these increased loads should be within the accepted norms of serviceability and strength for the masonry arch to be retained. In the current initiative, the Indian Railway is proposing to increase the axle loads on the track from the present level of 20.32 tons to either 25 tons or, in certain heavy haulage designated routes, to 30 tons. The 30 tons axle loads correspond to standard heavy mineral loads (HML). The CDA in Table 7 denotes the coefficient of dynamic augment. The design CDA values are defined in the Indian Railway Bridge Rules as are the allowable limits for deflections and stresses. The responses of the arch to the possible increased load conditions are also given in Table 7. It can be seen from this table that all the response quantities assessed are within the safe limits for the increased loading standards. The arch is thus deemed to be safe for the increased proposed loading and in this sense is satisfactory and in good condition.

5 Discussion

The reasonably good correspondence of the response time histories and the peak values given by the numerical model with the site data for a reasonably well-distributed number of response parameters, including strain values measured on the stone, provides confidence that the converged material properties obtained from the proposed model updating procedure are a good representation of those that exist in the field. The stone modulus is taken as virtually unchanged, as a value of 13.2 GPa for medium-grained sandstone is in accordance with what numerous researchers have considered. The value of 170 MPa estimated for the fill is again well within the range of expected values for this parameter. The E value of the concrete fill is estimated to be 3 GPa, which seems to be a reasonable value for this parameter. The value of the modulus of elasticity of mortar is estimated at 972 MPa, which shows some deterioration as compared to its expected value.

From the model updation procedure and the good convergence of the results of the finite element model with the site-measured data, it can be concluded that the finite element model used in this study is a good representation of the structure. Thus, the responses due to the possible future increased loading can be considered indicative of the "true" state of the responses. From the discussion earlier, the condition of the arch is thus estimated as being reasonably satisfactory. Several analyses were done using the updated numerical model for design loads that are considered to be used in Indian Railway codes in the future for heavily loaded routes, and the arch was found to be safe

Table 6 Final values of parameters

Parameter	Final value starting at relative minima	Final values (first pass) starting at boundary	From standard finite element software	Without formal optimization
Young's modulus—voussoir (GPA)	13.2	12.8	14.82	13.2
Young's modulus—basic fill (MPA)	170	200	108	120
Young's modulus—haunch fill (GPA)	3	2.3	1.15	1.4
Young's modulus of mortar (MPA)	972	972	1,833	865
Young's modulus—abutment fill	850 MPa	920 MPa	924 MPa	1.2 GPa
Error norm	0.070	0.084	0.145	0.18

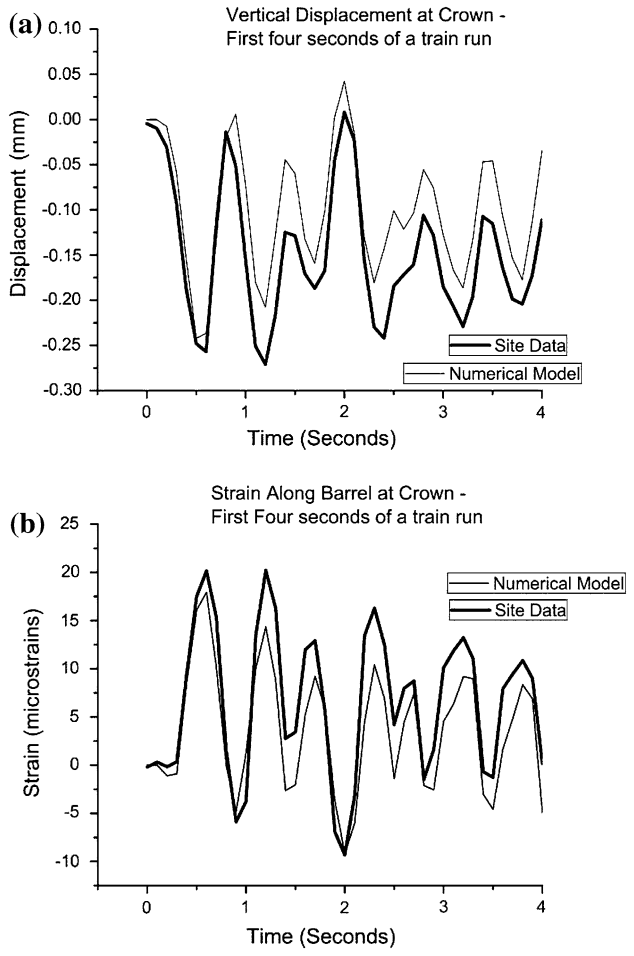

Fig. 11 Comparisons of response at crown of arch: (**a**) displacement and (**b**) strain

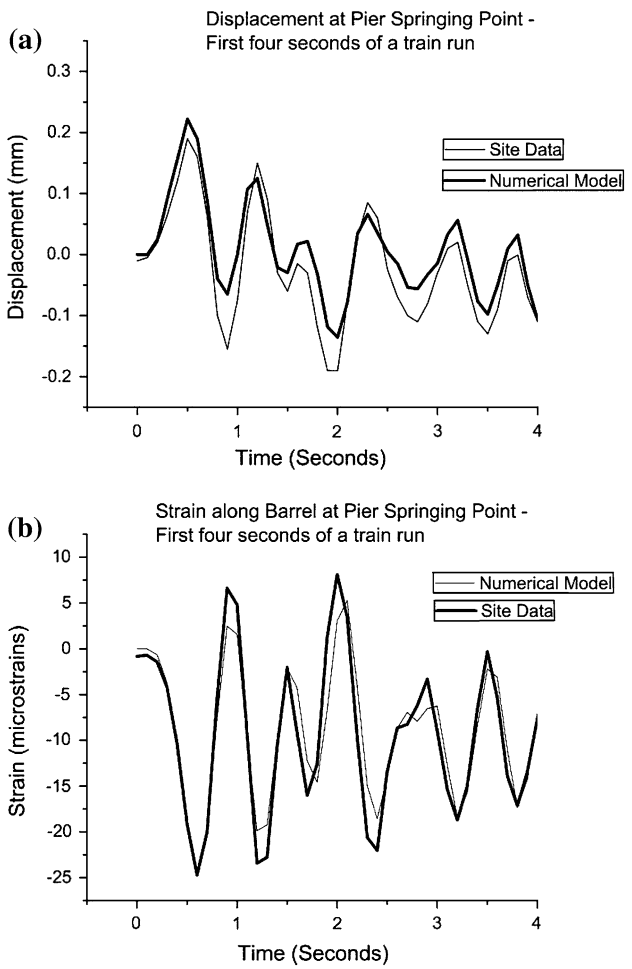

Fig. 12 Comparisons of response at pier side springing point: (**a**) displacement and (**b**) strain

from a design perspective. In fact, even if the full dynamic augment as specified in the current railway codes are considered in the analysis, it is seen that the arch is stressed to only about 60% of its allowable design stress value. It is thus surmised that the specific arch bridge considered can carry the increased design loads and no replacement or retrofit is needed at the current point of time. However, it must be noted that since the model updating procedure did show some deterioration in mortar properties, this should be monitored in the future to ensure that the failure of

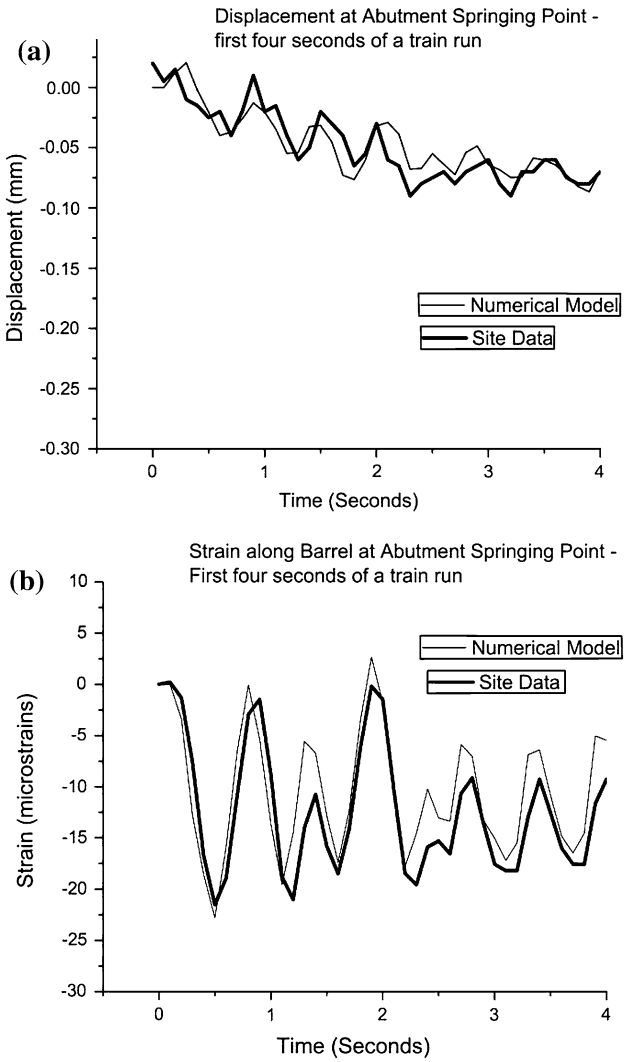

Fig. 13 Comparisons of response at abutment side springing point (**a**) displacement and (**b**) strain

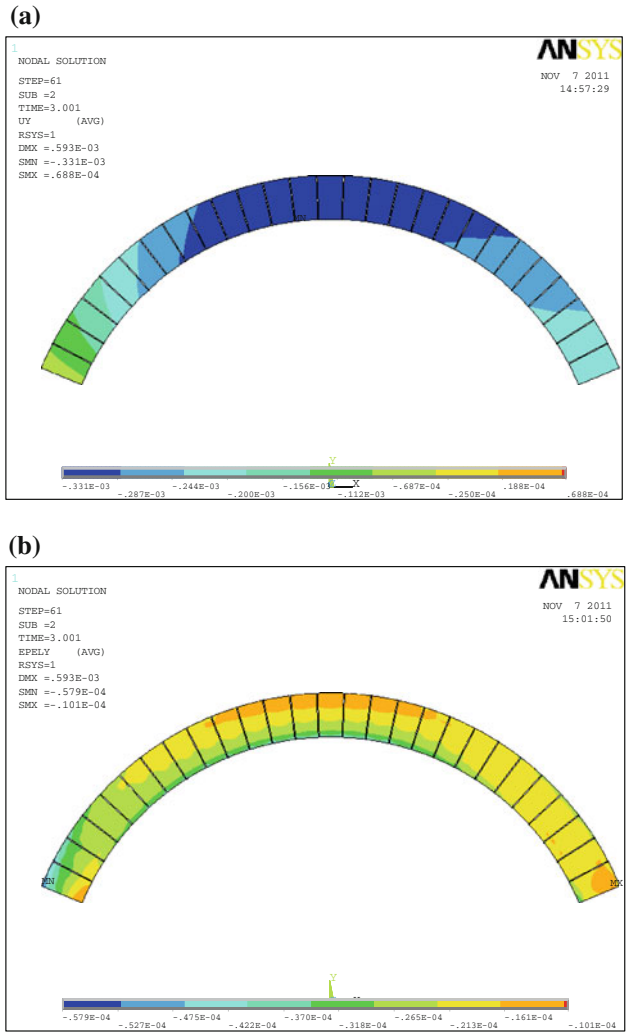

Fig. 14 Displacement and strain contours from finite element model at a particular time step: **a** displacement contours and **b** strain contours

Table 7 Comparison of design response values with allowable values

Loading standard	Units	A Self-weight	B Live load with design CDA	C Total A + B	D Live load with total CDA	E Total A + D	Allowable	Response location and type
25 ton HML	mm	0.09	−0.59	−0.50	−0.67	−0.58	−1.25	Crown displacement
		0.09	−0.66	−0.57	−0.76	−0.66		
25 ton HML	kg/cm^2	−8.5	−6.0	−14.5	−6.8	−15.4	−26.4/2.64	Crown longitudinal stress
		−8.5	−6.8	−15.3	−7.8	−16.3		
25 ton HML		1.1	−9.0	−7.9	−10.5	−9.4		Abutment longitudinal stress
		1.1	−9.7	−8.6	−11.2	−10.2		
25 ton HML		1.1	−9.0	−7.9	−10.5	−9.4		Pier longitudinal stress
		1.1	−9.7	−8.6	−11.2	−10.2		

mortar joints do not compromise the structural integrity of the bridge.

6 Conclusion

A novel model updating algorithm is proposed here that transforms a multi-parameter optimization problem into multiple reasonably tractable single or double parameter optimization problems based on some hierarchical rules, so that visual verification using two- or three-dimensional plots of the error sensitivity analysis is possible. The process followed was an algorithmic parametric identification technique, where the parameters were estimated in a least-squared error sense. It should be noted that the algorithm proposed is practical, based on a physical understanding of the parameters, for real masonry arch bridges, where data recorded from traffic on the bridge is used to update a finite element model of the bridge. It cannot be emphasized enough that the algorithm does not purport to be a new mathematical optimization algorithm. The efficacy and the robustness of the updating algorithm are illustrated, as it is shown to converge to identical optimized parameter values independent of the starting point, and it out-performs a standard multi-parameter algorithm incorporated in a standard finite element software package for the specific arch bridge considered in this study. It can be stated here that the developed updating algorithm has been used over various types of bridges having different response data sets. The only important criterion is that the responses used have to be sensitive to the structural parameters that are being updated.

The proposed algorithm numerically estimates values of displacements and strain response time histories that correspond well with recorded site data, and hence can be said to be a reliable procedure for condition assessment of masonry arch bridges. The cost of the monitoring and condition assessment exercise is nominal when compared with the cost, in terms of resources used and revenue lost, of replacing such a bridge based on its age. It can, therefore, be concluded that the proposed monitoring and condition assessment procedure for a masonry arch bridge has potential to be a robust technique for management of such bridges.

References

1. Ansys user's manual (1998) Swanson Analysis Systems
2. Audenaert A, Fanning P, Sobczak L, Peremans H (2008) 2-D analysis of arch bridges using an elasto-plastic material model. Eng Str 30:845–855
3. Bayraktar A, Altunisik AC, Birinci F, Sevim B and Turker T (2010) Finite element analysis and vibration testing of a two span masonry arch bridge. J Perform Constr Facil, ASCE 24(1):46–52
4. Boothby TE (2001) Analysis of masonry arches and vaults. Prog Struct Eng Mater 3:246–256
5. Cavicchi A, Gambarotta L (2006) Two-dimensional finite element upper bound limit analysis of masonry bridges. Comput Struct (84):2316–2328
6. Crisfield MA (1988) Numerical methods for the nonlinear analysis of bridges. Comput Struct 30(3):637–644
7. Day RW (2005) Foundation engineering handbook: design and construction with the 2006 international building code, McGraw Hill Construction, ASCE Press. ISBN: 0-07-144769-5
8. Fanning PJ, Boothby TE (2001) Three-dimensional modelling and full scale testing of stone arch bridges. Comput Struct 79:2645–2662
9. Ford TE, Augarde CE, Tuxford SS (2003) Modelling masonry arch bridges using commercial finite element software. 9th International Conference on Civil and Structural Engineering Computing, Egmond aan Zee, The Netherlands
10. Gilbert M (2007) Limit analysis applied to masonry arch bridges: state-of-the-art and recent developments, arch'07—5th international conference on arch bridges
11. Heyman J (1966) The stone skeleton. Int J Solids Struct 2:249–279
12. Jiang K, Esaki T (2002) Quantitative evaluation of stability changes in historical stone bridges in Kagoshima, Japan, by weathering. Eng Geol 63:83–91
13. Karantzikis MI (1997) Seismic analysis and design of integral bridges with soil–abutment interaction, Master thesis, Department of Civil Engineering, National Technical University of Athens (NTUA), Athens
14. Lukaszewski P (2003) Development of fracture processes in silesian carboniferous sandstones. Geol Quart 47(1):29–38
15. McNary WS, Abrams DP (1985) Mechanics of masonry in compression. J Struct Eng (ASCE) 111(4):857–870
16. Orban Z (2007) UIC project on assessment, inspection and maintenance of masonry arch railway bridges, arch 07—5th international conference on arch bridges
17. Pippard AJS, Baker JF (1943) The voussoir arch. In: The analysis of engineering structures 2nd edition. Edward Arnold and Company, London
18. Pippard AJS, Tranter E, Chitty L (1936) The mechanics of the voussoir arch. J Inst Civ Eng 4(2):281–306
19. Spyrakos CC (1992) Seismic behaviour of bridge piers including soil–structure interaction. Comput Struct 4(2):373–384
20. Tóth AR, Orbán Z, Bagi K (2009) Discrete element analysis of a stone masonry arch. Mech Res Commun 36:469–480